Journal of Solid State Chemistry 181 (2008) 2494–2500

Contents lists available at ScienceDirect

Journal of Solid State Chemistry

journal homepage: www.elsevier.com/locate/jssc

Type A–B carbonate chlorapatite synthesized at high pressure

Michael E. Fleet *, Xi Liu

Department of Earth Sciences, University of Western Ontario, London, Ontario, Canada N6A 5B7

ARTICLE INFO

Article history:
Received 24 March 2008
Received in revised form
6 June 2008
Accepted 10 June 2008
Available online 12 June 2008

Keywords:
Apatite structure
Chlorapatite
Carbonate ion
Biomineralization
Clathrates

ABSTRACT

Sodium-bearing type A–B carbonate chlorapatites {CCLAP; $Ca_{10-(y+z)}Na_y\square_z[(PO_4)_{6-(y+2z)}(CO_3)_{y+2z}][Cl_{2-2x}(CO_3)_x]$, with $x \approx y \approx 4z \approx 0.4$} have been synthesized from carbonate-rich melts at 1350–1000 °C and 1.0 GPa, and investigated by single-crystal X-ray structure and FTIR spectroscopy. Typical crystal and compositional data are: $a = 9.5321(4)$ Å, $c = 6.8448(3)$ Å, space group $P6_3/m$, $R = 0.027$, $R_w = 0.025$, $x = 0.37(3)$, $y = 0.57(2)$. Crystal-chemical features and FTIR spectra are similar to Na-bearing type A–B carbonate hydroxyapatites (CHAP) and fluorapatites (CFAP) reported recently. The molar amounts of Na and channel (type A) carbonate maintain a near 1:1 ratio in all three composition series, confirming that the Na cation and A and B carbonate ion substituents exist as a defect cluster within the apatite matrix, to facilitate charge compensation and spatial accommodation. Uptake of carbonate is significantly lower in CCLAP than in CHAP for similar conditions of crystal synthesis.

1. Introduction

The apatite-type structure is adopted by numerous inorganic compounds of general formula $M(1)_2M(2)_3(BO_4)_3X$, where $M(1)$ and $M(2)$ are large cations, B metalloids and X halides or oxy-anions [1,2]. The calcium phosphate apatite sub-group $[Ca(1)_4Ca(2)_6(PO_4)_6X_2]$ includes the common apatite minerals and mineral components, hydroxyapatite [HAP; ideally $Ca_{10}(PO_4)_6(OH)_2$; $Z = 1$], fluorapatite [FAP; $Ca_{10}(PO_4)_6F_2$] and chlorapatite [CLAP; $Ca_{10}(PO_4)_6Cl_2$], as well as carbonated hydroxyapatite (CHAP). Calcium phosphate apatites have importance in geochemistry, biology, agriculture, and materials science. Apatites are the ore minerals for phosphorus and agricultural phosphates, and they sequester rare-earth elements, actinides, and volatile elements in the Earth's crust and mantle. CHAP is by far the most important biomineral, accounting for up to about 65% of cortical bone and 97% of dental enamel [3]. Apatite minerals and compounds are actively researched in connection with diverse applications in orthopedic medicine and dentistry, containment of high-level nuclear waste, and the phosphor and laser industries.

Natural Ca apatites have the hexagonal space group $P6_3/m$, although pure, end-member HAP and CLAP crystallize in the monoclinic space group $P2_1/b$ [4]. In the hexagonal $P6_3/m$ structure, isolated PO_4 tetrahedra centered at $z = \frac{1}{4}, \frac{3}{4}$ are linked by Ca(1) in nine-fold (6+3) coordination and Ca(2) in an irregular seven-fold (6+1) coordination (Fig. 1). A prominent feature of the structure is the large c-axis channel which accommodates the X anion component (F, OH, Cl, CO_3, etc.). The apatite channel is defined by triclusters of Ca(2) cations at $z = \frac{1}{4}, \frac{3}{4}$. In FAP, the F anion is located on the c-axis at $z = \frac{1}{4}, \frac{3}{4}$ in the center of a tricluster of Ca(2). The hydroxyl ion in HAP and Cl in CLAP are displaced along the c-axis and have split atom positions with occupancy of 0.5: the hydroxyl oxygen is at $z = \pm(0.198, 0.302)$ and the much larger Cl anion is displaced further at $z = \pm(0.432, 0.068)$ [4]. Thus, the coordination of the X anion with Ca(2) is equilateral triangular in FAP but near octahedral in CLAP.

The structural role of the carbonate ion in CHAP and carbonated FAP (CFAP) has been investigated extensively by vibrational spectroscopy and X-ray powder and single-crystal and neutron powder diffraction methods [5–25]. The carbonate ion can be accommodated either in the c-axis structural channel or as a substituent for the phosphate group: the former carbonate is known as type A and the latter as type B. Detailed information on these two carbonate ion environments was obtained recently from X-ray structure study of CHAP and CFAP crystals grown from carbonate melts [19,20,22,24]. In addition, we found that Na, in amounts similar to that of apatite biominerals, promoted the introduction of carbonate. Moreover, the Na cation and A and B carbonate ions were locally coupled as a defect cluster within the apatite matrix, to facilitate charge compensation and minimize the effects of spatial accommodation. The molar proportions of Na and A and B carbonate ions were in the approximate ratios 1:1:1 in CHAP and 1:1:2 in CFAP.

These studies are presently extended to the accommodation of carbonate in Na-bearing carbonate chlorapatite (CCLAP), to investigate the influence of a large mononuclear anion in the

* Corresponding author. Fax: +1 519 661 3198.
E-mail address: mfleet@uwo.ca (M.E. Fleet).

0022-4596/$ - see front matter © 2008 Elsevier Inc. All rights reserved.
doi:10.1016/j.jssc.2008.06.016

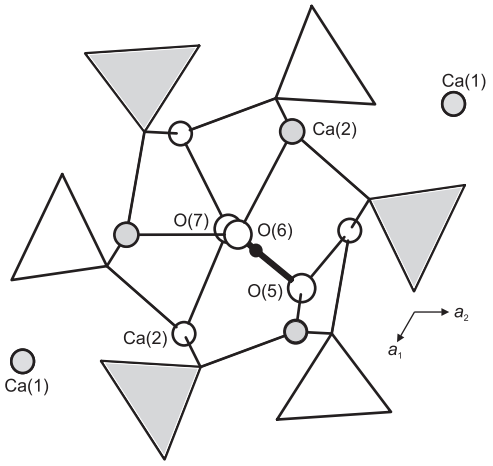

Fig. 1. Structure of carbonate chlorapatite (CCLAP), showing location of one of 12 possible orientations of the type A carbonate ion in apatite channel: unit-cell origin is in center of figure; shaded phosphate polyhedra and Ca(2) atoms are centered at $z = \frac{3}{4}$.

apatite channel on the uptake of carbonate. A further area of interest here is related to the displacement and mobility of channel anions in apatite structures, since it is well known that either large mononuclear anions (e.g., Cl^-) in the *X* site or large cations (e.g., Pb^{2+}) in the Ca(2) site result in displacement of the *X* anion from the ideal configuration of FAP [4,26].

2. Experimental procedures

Single crystals of carbonate-bearing chlorapatite (CCLAP) were prepared by direct reaction of analytical grade reagents ($Ca_2P_2O_7$, $CaCl_2$, $CaCO_3$, and Na_2CO_3) at high pressure and temperature using a Depths of the Earth Company Quick Press. A common starting composition (labeled Cl-1) was mixed in the stoichiometric proportion of the nominal type B carbonate chlorapatite composition $Ca_8Na_2[(PO_4)_4(CO_3)_2]Cl_2$ with 2 mol CO_2 in excess. Both calcium chloride ($CaCl_2$) and $Ca_2P_2O_7$ were heated at 700 °C and 1 atm for 24 h to remove water; $CaCO_3$ and Na_2CO_3 were dried at 200 °C and 1 atm for 48 h. $CaCl_2 \cdot 2H_2O$ reagent was previously heated at 300 °C and 1 atm for 24 h to prepare anhydrous $CaCl_2$. These prepared chemicals were mixed and ground under acetone in an agate mortar, and stored at 110 °C for later use. In addition, furnace parts were previously fired at 1000 °C in air. The starting mixture was encapsulated in a sealed platinum tube, with a diameter of 5 mm and a height of 10 mm, which was separated by crushable MgO tubing from a graphite sleeve. All experiments were quenched at pressure by switching off the furnace. Run conditions are summarized in Table 1, and were varied to investigate the effects of soaking temperature and cooling gradient in crystal growth. Five experiments were performed at high pressure (1 GPa), but only three yielded crystals of a size suitable for X-ray structure study. In addition, two experiments were performed at moderate pressures (0.13–0.21 GPa) using a hydrothermal apparatus and the Cl-1 starting mixture with and without an addition of 8 wt% HAP.

Products were characterized by optical microscopy, powder X-ray diffraction (Rigaku D/MAX-B rotating anode system; Co*K*α X-radiation), electron probe micro-analysis (EPMA; JEOL JXA-8600, using a lead stearate spectrometer crystal for carbon), and Fourier transform infrared (FTIR) spectroscopy (Nicolet Nexus 670 FTIR spectrometer). The infrared spectra were obtained for both hand-separated CCLAP crystals (LM169 and LM173) and bulk samples using KBr pellets (Figs. 2b, c and 3). About 10 mg of apatite crystal product was first ground to a powder, then diluted in an agate mortar with 1 g of KBr and ground under an infrared heating lamp to a grain size $<25\,\mu m$. Transparent pellets were made under vacuum at a pressure of 200 kg/cm^2. The temperature

Table 1
Synthesis experiments

Expt.	Starting mixture	*P* (GPa)	*T* (°C)	Time	Ramp (°C/min)	Product/crystal size
Hydrothermal experiments (days)						
LM166	Cl-1	0.21	950	0	−0.05	CCLAP/small
		0.13	500	4		
LM167	Cl-1+(8 wt% HAP)	0.21	950	0	−0.05	CCLAP/small
		0.13	500	4		
Piston-cylinder experiments (h)						
LM165	Cl-1	1.0	1250	31	–	CCLAP/small
LM168	Cl-1	1.0	1400	24	−2	CCLAP/small
			1200	48		
LM169	Cl-1	1.0	1350	24	–	CCLAP/large[a]
LM171	Cl-1	1.0	1350	7	−2	CCLAP/small
			1200	40		
LM173	Cl-1	1.0	1350	6	−0.1	CCLAP/medium
			1000	36		

[a] Up to 200 μm diameter.

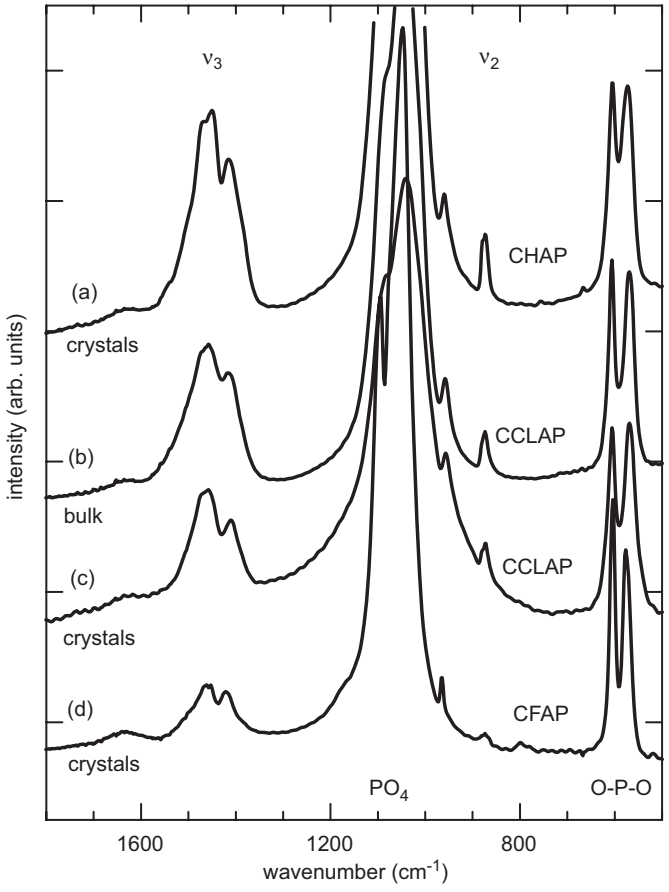

Fig. 2. Fourier transform infrared (FTIR) spectra for Na-bearing type A–B carbonate apatites synthesized at high *P–T*, identifying bands due to asymmetric stretching (ν_3) and out-of-plane bending (ν_2) of carbonate ions, as well as stretching and bending of phosphate: (a) CHAP, LM005 [22]; (b) and (c) CCLAP, LM169; (d) CFAP, LM130. Note that the spectra for (a), (c) and (d) were collected using hand-separated crystals: the hand-separated spectrum for LM173 is essentially identical to that for LM169; see text for band assignments and interpretation.

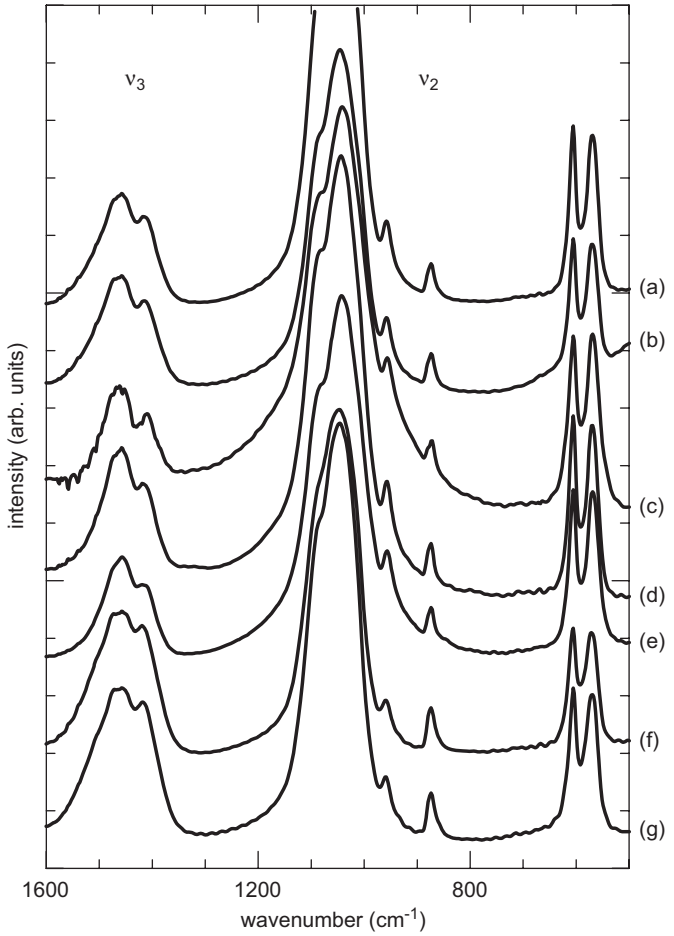

Fig. 3. Fourier transform infrared (FTIR) spectra for bulk samples of Na-bearing type A–B carbonate chlorapatites (CCLAP): (a) LM169; (b) LM165; (c) LM168; (d) LM171; (e) LM173; (f) LM166; and (g) LM167 (see Table 1 for conditions of synthesis).

Table 2
Experimental details for X-ray structures[a]

Experiment	LM169[b]	LM171	LM173
CCLAP crystal	xt399	xt400	xt402
Crystal size (mm^3)	$0.10 \times 0.11 \times 0.13$	$0.10 \times 0.05 \times 0.09$	$0.08 \times 0.08 \times 0.13$
Crystal shape	Prism	Tablet	Prism
a (Å)	9.5321(4)	9.5121(4)	9.5252(2)
c (Å)	6.8448(3)	6.8603(4)	6.8522(2)
Space group	$P6_3/m$	$P6_3/m$	$P6_3/m$
Formula weight	991.0	1012.9	963.1
Density (g/cm^3)	3.055	3.129	2.969
Reflections			
Unique	579	575	574
Number, with ($I<3\sigma_{(I)}$)	144	206	111
$R_{(I)}$	0.023	0.029	0.016
$R_{(I),w}$	0.038	0.043	0.030
Refined parameters	52	52	52
μ (cm^{-1})	28.6	29.6	27.5
R	0.027	0.030	0.033
R_w	0.025	0.025	0.026
S	1.33	1.13	1.93
g ($\times 10^4$)	1.1(1)	0.62(9)	1.3(1)
$\Delta\rho$ ($e\,Å^{-3}$) (+)	0.42	0.47	0.52
(−)	0.45	0.45	0.55

[a] X-ray diffraction measurements were made at room temperature and pressure.

[b] Formula amounts by EPMA: LM169—$Ca_{9.29}Na_{0.40}[(PO_4)_{5.55}(CO_3)_{0.51}][Cl_{1.39}(CO_3)_{0.31}]$; LM171—$Ca_{9.44}Na_{0.39}[(PO_4)_{5.62}(CO_3)_{0.35}][Cl_{1.36}(CO_3)_{0.32}]$; LM173—$Ca_{9.07}Na_{0.39}[(PO_4)_{5.43}(CO_3)_{0.74}][Cl_{1.33}(CO_3)_{0.34}]$.

of the sample under the infrared heating lamp was 60 ± 5 °C, and the exposure time was typically 10–30 min.

Single crystals from experiments LM169, LM171 and LM173 (Table 1) were evaluated for X-ray structure analysis by optical microscopy. Single-crystal measurements were made at room temperature and pressure with a Bruker–Nonius Kappa CCD diffractometer and graphite-monochromatized Mo$K\alpha$ X-radiation (50 kV, 32 mA, $\lambda = 0.7107$ Å). The COLLECT software [27] was used for unit-cell refinement and data collection. The reflection data were processed with SORTAV-COLLECT, using an empirical procedure for absorption correction, and SHELXTL/PC [28]. Structure refinements were made with LINEX77 [29]. Scattering factors for neutral atomic species and values of the anomalous scattering factors f' and f'' were taken, respectively, from Tables 2.2A and 2.3.1 of the International Tables for X-ray Crystallography [30]. Relevant experimental details are given in

Table 3
Positional and isotropic thermal parameters ($Å^2$) $U_{eq} = (1/3)\Sigma_i\Sigma_j\, U^{ij}\, a^i a^j\, a_i \cdot a_j$

	Site occupancy	x	y	z	U (U_{eq})
Experiment LM169 (xt399)					
Ca(1)	0.951(4)	2/3	1/3	0.00214(8)	0.0147(3)
Ca(2)	0.965(3)	0.99454(7)	0.25648(7)	0.25	0.0178(2)
P	0.905(4)	0.37094(9)	0.40238(9)	0.25	0.0106(2)
O(1)	0.905	0.4839(2)	0.3324(2)	0.25	0.0198(5)
O(2)	1.0	0.4642(2)	0.5869(2)	0.25	0.0286(5)
O(3)	0.905	0.2612(2)	0.3479(2)	0.0712(2)	0.0314(5)
Cl(1)	0.240(8)	0	0	0.382(1)	0.014(2)
Cl(2)	0.085(5)	0	0	0.301(2)	0.014
Cl(3)	0.222(5)	0	0	0.048(1)	0.014
C(1)	0.031	0.046[a]	0.065	0.492	0.025
O(5)	0.031(3)[b]	0.144	0.220	0.472	0.025
O(6)	0.031	0.005	0.002	0.662	0.025
O(7)	0.031	0.990	0.972	0.343	0.025
O(8)	0.048	0.311(4)	0.392(3)	0.443(4)	0.025
O(9)	0.095	0.511(2)	0.363(2)	0.25	0.025
Experiment LM171 (xt400)					
Ca(1)	0.950(4)	2/3	1/3	0.0020(1)	0.0158(4)
Ca(2)	0.971(4)	0.99335(8)	0.25527(8)	0.25	0.0197(3)
P	0.903(5)	0.3706(1)	0.4018(1)	0.25	0.0123(3)
O(1)	0.903	0.4831(3)	0.3312(3)	0.25	0.0196(7)
O(2)	1.0	0.4639(3)	0.5859(3)	0.25	0.0306(7)
O(3)	0.903	0.2603(2)	0.3469(3)	0.0719(3)	0.0324(6)
Cl(1)	0.251(9)	0	0	0.386(2)	0.015(3)
Cl(2)	0.110(5)	0	0	0.301(2)	0.015
Cl(3)	0.126(7)	0	0	0.048(2)	0.015
C(1)	0.038	0.046	0.065	0.492	0.025
O(5)	0.038(3)	0.144	0.220	0.472	0.025
O(6)	0.038	0.005	0.002	0.662	0.025
O(7)	0.038	0.990	0.972	0.343	0.025
O(8)	0.048	0.317(4)	0.395(4)	0.442(4)	0.025
O(9)	0.097	0.511(2)	0.363(2)	0.25	0.025
Experiment LM173 (xt402)					
Ca(1)	0.954(4)	2/3	1/3	0.00208(9)	0.0156(3)
Ca(2)	0.969(3)	0.99419(7)	0.25605(7)	0.25	0.0191(2)
P	0.906(4)	0.37109(9)	0.40243(9)	0.25	0.0118(2)
O(1)	0.906	0.4838(2)	0.3322(2)	0.25	0.0203(5)
O(2)	1.0	0.4642(2)	0.5867(2)	0.25	0.0297(5)
O(3)	0.906	0.2611(2)	0.3480(2)	0.0712(2)	0.0320(5)
Cl(1)	0.271(8)	0	0	0.388(1)	0.016(2)
Cl(2)	0.091(5)	0	0	0.302(2)	0.016
Cl(3)	0.168(6)	0	0	0.048(1)	0.016
C(1)	0.035	0.046	0.065	0.492	0.025
O(5)	0.035(3)	0.144	0.220	0.472	0.025
O(6)	0.035	0.005	0.002	0.662	0.025
O(7)	0.035	0.990	0.972	0.343	0.025
O(8)	0.047	0.314(3)	0.394(3)	0.443(4)	0.025
O(9)	0.094	0.512(2)	0.363(2)	0.25	0.025

[a] x, y, z for C(1), O(5) and O(6) are from Ref. [22].

[b] Multiplicity of O(5) and O(8) is 12 (equipoint 12i), whereas that of O(9) is 6 (equipoint 6h).

Table 4
Comparison of anisotropic displacement parameters

Position	Sample	U_{11}	U_{22}	U_{33}	U_{12}	U_{13}	U_{23}
Ca(1)	LM169	0.0175(5)	0.0175	0.0089(4)	0.0088	–	–
	LM171	0.0181(5)	0.0181	0.0113(5)	0.0090	–	–
	LM173	0.0183(5)	0.0183	0.0103(4)	0.0091	–	–
Ca(2)	LM169	0.0166(4)	0.0202(4)	0.0150(3)	0.0081(3)	–	–
	LM171	0.0174(4)	0.0226(4)	0.0176(4)	0.0090(3)	–	–
	LM173	0.0174(3)	0.0216(4)	0.0168(3)	0.0086(3)	–	–
P	LM169	0.0114(4)	0.0126(4)	0.0097(4)	0.0075(3)	–	–
	LM171	0.0126(5)	0.0143(5)	0.0117(5)	0.0081(4)	–	–
	LM173	0.0123(4)	0.0134(4)	0.0113(4)	0.0077(3)	–	–
O(1)	LM169	0.021(1)	0.026(1)	0.018(1)	0.016(1)	–	–
	LM171	0.021(1)	0.023(1)	0.020(1)	0.015(1)	–	–
	LM173	0.021(1)	0.025(1)	0.020(1)	0.016(1)	–	–
O(2)	LM169	0.022(1)	0.022(1)	0.042(1)	0.011(1)	–	–
	LM171	0.025(1)	0.023(1)	0.044(2)	0.012(1)	–	–
	LM173	0.025(1)	0.023(1)	0.043(1)	0.012(1)	–	–
O(3)	LM169	0.024(1)	0.053(1)	0.0258(9)	0.0257(9)	−0.0117(7)	−0.0213(8)
	LM171	0.024(1)	0.054(1)	0.027(1)	0.025(1)	−0.0113(9)	−0.020(1)
	LM173	0.025(1)	0.053(1)	0.0262(9)	0.0252(9)	−0.0112(7)	−0.0199(8)

Table 5
Selected bond distances (Å) and angles (deg)

		LM169 xt399	LM171 xt400	LM173 xt402
Ca(1)–O(1)	×3	2.428(1)	2.430(2)	2.429(1)
Ca(1)–O(2)^{I}	×3	2.462(1)	2.464(2)	2.463(1)
Ca(1)–O(3)^{I}	×3	2.805(2)	2.807(2)	2.802(2)
Mean		2.565	2.567	2.565
Ca(2)–O(1)^{II}		2.756(2)	2.732(2)	2.750(2)
Ca(2)–O(2)^{III}		2.309(2)	2.317(2)	2.311(2)
Ca(2)–O(3)^{IV}	×2	2.550(2)	2.547(2)	2.551(2)
Ca(2)–O(3)^{V}	×2	2.339(1)	2.344(2)	2.341(2)
Mean		2.474	2.472	2.474
Ca(2)–Cl(1)		2.630(2)	2.631(4)	2.643(3)
P–O(1)		1.525(2)	1.522(2)	1.523(2)
P–O(2)		1.523(2)	1.517(2)	1.520(2)
P–O(3)	×2	1.523(2)	1.522(2)	1.524(2)
Mean		1.523	1.521	1.523
O(1)–P–O(2)		111.9(1)	112.0(1)	112.0(1)
O(1)–P–O(3)	×2	111.46(7)	111.37(9)	111.49(7)
O(2)–P–O(3)	×2	107.38(9)	107.5(1)	107.30(9)
O(3)–P–O(3)^{VI}		107.0(1)	106.7(2)	107.0(1)

Notes: (I) $1-x, 1-y, -z$; (II) $1-y, x-y, z$; (III) $1-x+y, 1-x, z$; (IV) $1+x, y, z$; (V) $1+x-y, x, -z$; (VI) $x, y, \frac{1}{2}-z$.

Table 2, final parameters in Tables 3 and 4, and selected bond distances in Table 5.

3. Results and discussion

3.1. Experimental products

The products of the synthesis experiments listed in Table 1 were dominated by sodium- and carbonate-bearing chlorapatite (CCLAP) with minor amounts of quench carbonates. CCLAP was present in two grain sizes, as larger prismatic crystals up to 200 μm in length in experiment LM169 and as a fine-grained matrix. Experiments LM169 and LM173 produced sufficient large- and medium-sized crystals to separate crystal samples for FTIR spectroscopy (e.g., Fig. 2c). In addition, FTIR spectra were obtained for all products in bulk form (Fig. 3). Crystal size showed a broad correlation with soaking temperature and time (Table 1), with crystallization under near-liquidus conditions yielding the largest crystals. Single crystals from LM169, LM171 and LM173 were selected for X-ray structure analysis. Their EPMA compositions, given in terms of formula amounts in the footnote to Table 2, are similar and seemingly independent of variation in cooling gradient and final soaking temperature. The contents of Na and carbonate in these CCLAP crystals are intermediate between those of the carbonate fluorapatite (CFAP) and hydroxyapatite (CHAP; experiment LM005) studied earlier [22,24].

3.2. FTIR spectroscopy

The FTIR spectra (Figs. 2b, c and 3) are dominated by a complex band at about 1000–1100 cm^{-1} for the asymmetric stretch vibration of the phosphate group. In addition, they reveal very broad bands for molecular water at about 3300–3600 (OH stretch) and 1600–1700 cm^{-1} (H_2O in-plane bend), and bands for carbonate at 1400–1500 cm^{-1} (asymmetric stretch vibration; ν_3) and 873–880 cm^{-1} (out-of-plane bend vibration; ν_2). The characteristic band for the stretch vibration of structurally bound OH, which is near 3573 cm^{-1} in hydroxyapatite, is absent, as are features consistent with the presence of the HPO_4^{2-} ion [8,10]. Interpretation of the ν_3 carbonate band in the FTIR spectra of apatites with multiple carbonate species is complicated by band overlap and asymmetry of the doublet for the channel (type A) carbonate species [25]. Band overlap in the 1470–1450 cm^{-1} interval is particularly troublesome. Earlier studies on synthetic Na-free CHAP found that type A carbonate was characterized by a doublet band at about 1545 and 1460–1450 cm^{-1} (ν_3) and a singlet band at about 880–878 cm^{-1} (ν_2), whereas type B carbonate has these bands at about 1450–1455, 1410–1420 and 873–871 cm^{-1}, respectively [3,5,6,25,31]. However, Fleet and Liu [22,24] found recently that in synthetic Na-bearing A–B CHAP and A–B CFAP the ν_3 doublet for type A carbonate is apparently shifted to lower wavenumber into the region normally associated with type B carbonate. The present spectra for the Na-bearing CCLAP crystals have the same overall form in the ν_3 region as the CHAP spectra of Fleet and Liu [22] with resolved features at 1416, 1457, 1465, and 1471 cm^{-1}. The high wavenumber components are weaker than in the spectra of CHAP, consistent with more type B carbonate than type A (Fig. 2). However, the relative enrichment in type B is less than that reported for Na-bearing CFAP [24] (Fig. 2d). In agreement with these qualitative observations, fitted band areas for the 873 cm^{-1} (type B carbonate) and 880 cm^{-1} (type A) components of the compound band for the out-of-plane bend vibration (ν_2) yielded B/A ratios greater than unity (1.43, 1.49; Table 6) and generally intermediate between the values for CHAP (0.9) and CFAP (1.5, 2.2). The FTIR band areas of the carbonate vibration modes are consistently higher for bulk samples than for crystal samples (e.g., Fig. 2b and c), showing that more carbonate is incorporated in quench CCLAP than in CCLAP grown under equilibrium conditions. Nevertheless, the B/A ratios from the ν_2 band are essentially constant in both crystals and bulk samples (Table 6), showing that the crystal structures of high-temperature near-liquidus and quench (or low-temperature) CCLAP crystals must be similar.

The composite ν_3 band in IR spectra of Na-bearing carbonate apatites under-represents the proportion of type A carbonate, when the band assignments from synthetic Na-free apatites are used as reference. The weak and diffuse intensity beyond 1500 cm^{-1} could represent multiple channel sites for carbonate

Table 6
Carbonate contents and oxygen–oxygen distances

Experiment	LM169 xt399	LM171 xt400	LM173 xt402
Final temperature (°C)	1350	1200	1000
EPMA			
Sodium (pfu)[a]	0.40(4)	0.39(3)	0.39(5)
X-ray structure			
A carbonate (pfu)	0.37(3)	0.46(4)	0.42(3)
B carbonate (pfu)	0.57(2)	0.58(3)	0.57(2)
Molar B/A	1.55	1.28	1.35
FTIR B/A (v_2-crystals)	1.49	–	1.43
FTIR B/A (v_2-bulk)[b]	1.55	1.57	1.42
O–O distances for B carbonate ion (Å)			
O(8)–O(2)	2.15(2)	2.11(3)	2.13(2)
O(2)–O(9)	2.39(2)	2.37(3)	2.39(2)
O(9)–O(8)	2.44(4)	2.41(4)	2.44(4)

[a] pfu is per formula unit.
[b] B/A for bulk samples of other experiments were: LM165—1.37; LM168—1.43; LM166—1.91; LM167—1.62.

ions [8,20,25] (which do not seem to be supported by the X-ray structures for Na-bearing CHAP, CFAP and CCLAP), multiple Ca(2) site configurations for a single type A carbonate site, or destabilization of the A carbonate ion in close proximity to the channel wall. Certainly, it is not possible to deconvolute these spectra without further crystal-chemical insight. In contrast, the complex v_2 band appears to better reflect the true proportions of the principal carbonate species. In biological apatites this region is normally deconvoluted to give singlet bands at 878 cm^{-1} (type A carbonate), 871 cm^{-1} (type B carbonate), and 866 cm^{-1} (labile carbonate) [7,8]. Rey and coworkers reported B/A ratios from v_2 region spectra ranging from 1.1 to 0.8 for pig enamel [8] and 1.4 to 1.2 for various bone samples, including cow, human, chicken, rat, and rabbit [8,10]. Evidently, these biominerals are all type A–B carbonate hydroxyapatites, and very similar in composition and structure to synthetic Na-bearing CHAP [22].

Although we have not extracted quantitative information from the composite v_3 band, this spectral region does have an important qualitative application. The overall profile of the v_3 band is essentially the same for all samples of Na-bearing CCLAP studied, as well as for all samples of Na-bearing CHAP and CFAP of previous studies [22,24] (Figs. 2 and 3). Thus, the v_3 band profile is independent of composition series (X=OH, F, Cl) and amount of Na and carbonate present. This clearly indicates that the local stereochemical environment of the carbonate substituents is the same in all Na-bearing carbonate apatites, and complements evidence from chemical compositions and X-ray structures pointing to the local clustering of Na and A and B carbonate in the host apatite matrix (Figs. 4 and 5).

3.3. X-ray structures

The single crystals from experiments LM169, LM171 and LM173 were of high diffraction quality (e.g., Table 2). Their diffraction patterns were consistent with space group $P6_3/m$ and revealed no evidence of ordering of the carbonate ion defects in the form of superstructure reflections, diffuse scattering or anomalous reflection broadening. Although the Na and carbonate ion substituents are disordered within the host Ca apatite structure, they are replicated in the average structure by the hexagonal $P6_3/m$ symmetry and therefore contribute coherent Bragg scattering intensity to the single-crystal diffraction pattern. In addition, atoms of the host structure are locally displaced to accommodate the carbonate ions, and this displacement results in

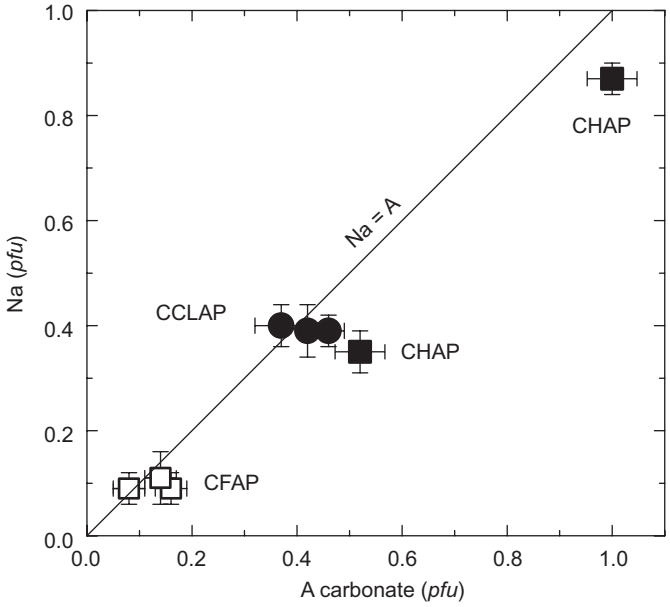

Fig. 4. Near linear 1:1 correlation of Na and type A carbonate in carbonate-bearing hydroxyapatite (CHAP; full squares) [22], fluorapatite (CFAP; open squares) [24], and chlorapatite (CCLAP; full circles): pfu is per formula unit ($Z = 1$).

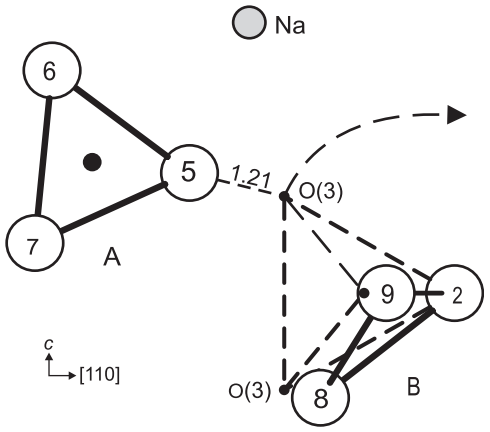

Fig. 5. Fragment of structure of CCLAP, showing location of B carbonate ion close to the sloping faces of a substituted phosphate tetrahedron: multiplicities due to $P6_3/m$ symmetry of the host apatite structure are not shown. Note that the symmetry-related O(3) oxygen is removed to avoid short interaction with O(5) of the proximal type A carbonate ion: elevation view; interatomic distance is Å.

anomalous increase in anisotropic displacement parameters [16,25]. Thus, X-ray structures of carbonate apatites present numerous challenges in interpretation, especially where carbonate contents are very low, as in the recent study of Na-bearing CFAP [24]. In particular, electron densities which may be appreciably less than that of a hydrogen atom and overlap of carbonate and host structure atoms limit the amount of structural information that can be extracted from X-ray structure analysis.

The three X-ray structure refinements generally followed previous studies [20,22,24,25] and yielded essentially the same ideal (carbonate-free) hexagonal CCLAP structure (Tables 3–5). Preliminary refinements started with ideal CCLAP stoichiometry. Weak peaks in residual electron density maps located oxygen atoms of the carbonate ions in the apatite channel (type A) and in the vicinity of the phosphate group (type B). Various constraints were added to promote convergence of the structure refinements, as detailed in Table 3. The scattering factors and dispersion

corrections for the Ca(1) and Ca(2) positions were weighted in proportion to the formula amounts of Ca and Na given in Table 2. The structure refinements confirmed that Ca(1) and Ca(2) were essentially fully occupied by (Ca+Na), but refinement of the individual site occupancies was ambiguous due to the minor content of Na and vacancies. Therefore, Ca(1) and Ca(2) occupancies were fixed at 1.0, with the small proportion of large cation site vacancies being ignored. The occupancy of P was less than unity, consistent with substitution of the phosphate group by the type B carbonate ion. It is well known that the phosphorus site occupancy yields the most reliable estimate of the extent of substitution by type B carbonate [13,16,32]. Therefore, the unit-cell contents were constrained according to: O(1) = P; and O(8) = O(9) = (6–P). The atom positions of the channel (type A) carbonate ion [C(1), O(5), O(6), and O(7)] were taken from the CHAP structure of sample LM005 in Fleet and Liu [22], and were not further refined (Fig. 1). The oxygen O(5), which was furthest away from the *c*-axis (Fig. 1) and least affected by the presence of chloride anions in the apatite channel was used for the occupancy refinement. Also, for all three crystals investigated, the residual electron density peaks consistent with O(5) were present in difference Fourier maps compiled after refinement of the structure with ideal carbonate-free stoichiometry. Finally, three separate sites were located for the electron density of the chloride anion in the apatite channel (Table 3).

3.4. Crystal chemistry

The X-ray structures confirm that the present Na-bearing CCLAP crystals are type A–B carbonate apatites, with contents of Na and A and B carbonate approximately intermediate between those of Na-bearing CHAP and CFAP [22,24] (Fig. 4) and essentially independent of the precise conditions of synthesis (Tables 1 and 6). Formula amounts of Na and A carbonate are consistent with the near linear (1:1) correlation reported for CHAP and CFAP (Fig. 4). This agreement for all three composition series is strong evidence that Na has an active role in the substitution of carbonate into the apatite channel, even though it does not appear in the usual charge-balanced substitution scheme: i.e.,

$$[^{A}CO_3 = 2Cl] \quad (1)$$

On the other hand, the molar B/Na ratio is greater than unity (approximately 1:1.5) and intermediate between the values for CHAP (1.0) and CFAP (2.0). Thus, the substitution of B carbonate into CCLAP and CFAP is more complex than the simple mechanism proposed for CHAP [22]:

$$[Na + {}^{B}CO_3 = Ca + PO_4] \quad (2)$$

Following discussion of CFAP [24], additional charge-balancing by vacancies at large cation sites:

$$[0.5\square + {}^{B}CO_3 = 0.5Ca + PO_4] \quad (3)$$

results in an overall substitution formula of $Ca_{10-(y+z)}Na_y\square_z[(PO_4)_{6-(y+2z)}(CO_3)_{y+2z}][Cl_{2-2x}(CO_3)_x]$, with $x \approx y \approx 4z \approx 0.4$. The small fraction of vacancies is undetectable by present methods and was ignored in the structure refinements.

The B carbonate ion was located close to the sloping (i.e., inclined to *c*-axis) faces of the substituted phosphate tetrahedron, in the configuration of CHAP, with one O(3) oxygen displaced to O(8) and the symmetry-related O(3) omitted (Fig. 5). The O(1) oxygen atom is displaced slightly to O(9) and the third B carbonate oxygen is concealed by the electron density of O(2). Our various studies on the average structures of CHAP, CFAP and CCLAP have failed to detect any significant residual electron density in the vicinity of the phosphate group except for that associated with B carbonate ions lying close to sloping faces [14,20,24]. The carbonate-for-phosphate substitution uses only three of the phosphate oxygen sites, and the local coupling of A and B carbonate ions dictates that the omitted oxygen is the symmetry-related O(3) atom; close proximity of the A and B carbonate ions would otherwise result in a prohibitively close O(5)–O(3) distance of 1.21 Å (Fig. 5). Logically, charge balance requirements favor placing the Na cation closest to this vacant O(3) oxygen site. The resulting oxygen–oxygen distances for the B carbonate ion (Table 6) are in satisfactory agreement with that for the ideal carbonate ion geometry (e.g., 2.219 Å in calcite) [33] and consistent with previous X-ray structure studies on type A–B CHAP and CFAP [20,22,24,25]. Discrepancies with the ideal O–O distance represent errors in locating atom positions in structures determined at the lower limit of resolution of the X-ray structure method using conventional laboratory equipment and do not imply that the carbonate ion geometries in CFAP are anomalously distorted.

In summary, studies on three separate composition series of carbonate apatite crystals grown in the presence of excess sodium carbonate, including CHAP [22], CFAP [24], and CCLAP, have yielded essentially the same environments for the A and B carbonate ions. These studies encompass a wide range in A and B carbonate content, extending from 0.1 to 0.2 pfu in CFAP, to 0.4–0.6 pfu in CCLAP, and up to 1.0 pfu in CHAP. The similar profiles of ν_3 bands in FTIR spectra for all carbonate apatite composition series and carbonate contents investigated (Figs. 2 and 3) together with the common X-ray structure suggest that the Na cation and A and B carbonate ion substituents are present as randomly distributed defect clusters within the host apatite structure. The defect cluster depicted in Fig. 5 facilitates local charge compensation by Na-for-Ca substitution, explains the linear 1:1 correlation between Na and A carbonate, and minimizes the effects of spatial accommodation. Charge compensation through the introduction of large cation site vacancies (substitution mechanism 3) in CFAP and CCLAP, which both have molar (B/Na) > 1, may involve a separate defect cluster, although this is not reflected in the ν_3 band profiles of these apatites (e.g. Fig. 2). It is possible that there exists a degree of intermediate range order, with several A–B pairs organized into columnar *c*-axis domains, analogous to the columnar domains suggested for mixed *X* anion occupancy in Ca apatites [4,7]. However, the X-ray diffraction patterns of these apatites do not reveal any evidence of extensive ordering and it seems unlikely that compositionally distinct domains analogous to those observed in Brazilian gem-grade apatite [34] exist in them.

Moreover, extensive intermediate range ordering is not consistent with the observed distribution of Cl in the apatite channel of CCLAP. In hexagonal $P6_3/m$ CLAP, Cl is displaced along the *c*-axis from the center of the tricluster of Ca(2) cations to the split atom position at $z = \pm(0.432, 0.068)$ to optimize the Cl–Ca(2) bond distance [4]. In Na-bearing CCLAP, Cl is more widely distributed along the *c*-axis, with at least three sites recognized (at *z* coordinates of about 0.382, 0.301, and 0.452; Table 3). The total Cl contents from the structure refinements (0.97–1.09 pfu) are somewhat less than the corresponding EPMA values (1.33–1.39 pfu; Table 2). This suggests that the electron density of Cl is actually smeared along *c*-axis and, in consequence, not all of it has been recovered. Evidently, Cl anions are readily displaced by the introduction of the bulky carbonate ions into the apatite channel, and their smeared distribution is evidence for considerable disorder of the two ionic species. If there were extensive ordered domains of hexagonal CLAP structure, the *z* coordinate of Cl in the average structure would be close to the end-member value. Displacement of the Cl anion along the *c*-axis to create a second Cl site has been reported previously for binary and ternary

solid solutions of Ca apatites (X=Cl, OH, F) [35,36], but with concomitant displacement of the Ca(2) triclusters to create a second Ca(2) site. However, there is no indication of a split site for Ca(2) in the present CCLAP structures (Tables 2–4). Displacement of the X anion in the apatite structure also occurs for very large $M(2)$ cations, e.g., in lead fluorapatite, the z coordinate of F is 0.453 and solid solutions with strontium fluorapatite result in a progressive linear shift towards the strontium end-member value of 0.25 [26]. Similarly, the OH oxygen of lead hydroxyapatite is displaced to near $z = 0.5$, but shifts progressively towards $z = 0.25$ with progressive Ca-for-Pb and Cd-for-Pb substitution [37,38].

Acknowledgments

We thank Michael Jennings for collection of the X-ray reflection data, Penny King for use of the FTIR equipment, and the Natural Sciences and Engineering Research Council of Canada for financial support.

Appendix A. Supplementary Materials

Supplementary data associated with this article can be found in the online version at doi:10.1016/j.jssc.2008.06.016.

References

[1] Y. Pan, M.E. Fleet, in: M.J. Kohn, J. Rakovan, J.M. Hughes (Eds.), Phosphates: Geochemical, Geobiological and Material Importance, Reviews in Mineralogy and Geochemistry, vol. 48, Mineralogical Society of America, Washington, 2002, pp. 13–49.
[2] T.J. White, C. Ferraris, J. Kim, S. Madhavi, in: G. Ferraris, S. Merlino (Eds.), Micro- and Meso-porous Mineral Phases, Reviews in Mineralogy and Geochemistry, vol. 57, Mineralogical Society of America and the Geochemical Society, Washington, 2005, pp. 307–373.
[3] J.C. Elliott, in: M.J. Kohn, J. Rakovan, J.M. Hughes (Eds.), Phosphates: Geochemical, Geobiological and Material Importance, Reviews in Mineralogy and Geochemistry, vol. 48, Mineralogical Society of America, Washington, 2002, pp. 427–453.
[4] J.M. Hughes, M. Cameron, K.D. Crowley, Am. Mineral. 74 (1989) 870–876.
[5] G. Bonel, Ann. Chim. (Paris) 7 (1972) 65–88.
[6] R.Z. LeGeros, O.R. Trautz, E. Klein, J.P. LeGeros, Experimentia 25 (1969) 5–7.
[7] C. Rey, B. Collins, T. Goehl, I.R. Dickson, M.J. Glimcher, Calcif. Tissue Int. 45 (1989) 157–164.
[8] C. Rey, V. Renugopalakrishnan, M. Shimizu, B. Collins, M.J. Glimcher, Calcif. Tissue Int. 49 (1991) 259–268.
[9] J.C. Elliott, Structure and Chemistry of the Apatites and other Calcium Orthophosphates, Elsevier, Amsterdam, 1994.
[10] H.-M. Kim, C. Rey, M.J. Glimcher, Calcif. Tissue Int. 59 (1996) 58–63.
[11] Y. Suetsugu, Y. Takahashi, F.P. Okamura, J. Tanaka, J. Solid State Chem. 155 (2000) 292–297.
[12] T.I. Ivanova, O.V. Frank-Kamenetskaya, A.B. Kol'tsov, V.L. Ugolkov, J. Solid State Chem. 160 (2001) 340–349.
[13] R.M. Wilson, J.C. Elliott, S.E.P. Dowker, Am. Mineral. 84 (1999) 1406–1414.
[14] R.M. Wilson, J.C. Elliott, S.E.P. Dowker, R.I. Smith, Biomaterials 25 (2004) 2205–2213.
[15] R.M. Wilson, S.E.P. Dowker, J.C. Elliott, Biomaterials 27 (2006) 4682–4692.
[16] Th. Leventouri, B.C. Chakoumakos, H.Y. Moghaddam, V. Perdikatsis, J. Mater. Res. 15 (2000) 511–517.
[17] Th. Leventouri, B.C. Chakoumakos, N. Papanearchou, V. Perdikatsis, J. Mater. Res. 16 (2001) 2600–2606.
[18] A. Antonakos, E. Liarokapis, T. Leventouri, Biomaterials 28 (2007) 3043–3054.
[19] M.E. Fleet, X. Liu, J. Solid State Chem. 174 (2003) 412–417.
[20] M.E. Fleet, X. Liu, J. Solid State Chem. 177 (2004) 3174–3182.
[21] M.E. Fleet, X. Liu, Biomaterials 26 (2005) 7548–7554.
[22] M.E. Fleet, Xi Liu, Biomaterials 28 (2007) 916–926.
[23] M.E. Fleet, Xi Liu, Am. Mineral. 92 (2007) 1764–1767.
[24] M.E. Fleet, Xi Liu, Am. Mineral. (2008), in press.
[25] M.E. Fleet, X. Liu, P.L. King, Am. Mineral. 89 (2004) 1422–1432.
[26] B. Badraoui, A. Aissa, A. Bigi, M. Debbabi, M. Gazzano, J. Solid State Chem. 179 (2006) 3065–3072.
[27] Nonius, COLLECT Software. Bruker–Nonius, Delft, The Netherlands, 1997.
[28] Siemens SHELXTL PC, Version 4.1, Siemens Analytical X-ray Instruments, Inc., Madison, WI, USA, 1993.
[29] P. Coppens, LINEX77, State University of New York, Buffalo, USA, 1977.
[30] J.A. Ibers, W.C. Hamilton (Eds.), International Tables for X-ray Crystallography, vol. IV, Kynoch Press, Birmingham, UK, 1974.
[31] J.C. Elliott, in: R.W. Fearnhead, M.V. Stack (Eds.), Tooth Enamel: Its Composition, Properties, and Fundamental Structure, John Wright & Sons, Bristol, UK, 1964, pp. 20–22.
[32] H. Morgan, R.M. Wilson, J.C. Elliott, S.E.P. Dowker, P. Anderson, Biomaterials 21 (2000) 617–627.
[33] J.R. Smyth, D.L. Bish, Crystal Structures and Cation Sites of the Rock-Forming Minerals, Allen & Unwin, London, 1988.
[34] C. Ferraris, T.J. White, J. Plévert, R. Wegner, Phys. Chem. Minerals 32 (2005) 485–492.
[35] J.M. Hughes, M. Cameron, K.D. Crowley, Am. Mineral. 75 (1990) 295–304.
[36] K. Sudarsanan, R.A. Young, Acta Crystallogr. B 34 (1978) 1401–1407.
[37] A. Bigi, M. Gandolfi, M. Gazzano, A. Ripamonti, N. Roveri, S.A. Thomas, J. Chem. Soc. Dalton Trans. (1991) 2883–2886.
[38] B. Badraoui, A. Bigi, M. Debbabi, M. Gazzano, N. Roveri, R. Thouvenot, Eur. J. Inorg. Chem. (2001) 1261–1267.